

Probe-assisted Depopulation Pumping in Low-pressure Alkali-metal Vapor Cells for Magnetometry

M. E. Limes,* J. Smoot, J. Perez, J. Freeman, C. Amano-Dolan, and D. Peters
National Security Institute, Virginia Tech, Blacksburg, VA, 24061, USA

W. Lee

Department of Physics, Harvard University, Cambridge, MA, 02138, USA

(Dated: February 12, 2026)

For precision atomic magnetometry, inert buffer gas is included in alkali-metal vapor cells to significantly broaden hyperfine transitions, which facilitates optical pumping and reduces diffusive relaxation, while also providing non-radiative excited state quenching. We show low-buffer gas pressure (below 50 Torr) alkali vapor cells with resolved hyperfine manifolds can also yield high-performance magnetometers. For high polarization in ^{87}Rb , we optically pump $F = 2$ states with narrow linewidth σ_+ light, while tuning a probe beam to depopulate $F = 1$ states ($\Delta\nu = 6.8$ GHz from $F = 2$). The probe tuning then also provides $F = 2$ detection with high optical rotation and low probe broadening; we demonstrate top-bottom gradiometry, within a single 25 Torr, 0.5 cc cell, that yields an Earth's field free-precession magnetometer sensitivity of $18 \text{ fT}/\sqrt{\text{Hz}}$ with a 1 kHz bandwidth, as well as RF magnetometer sensitivity of $12 \text{ fT}/\sqrt{\text{Hz}}$ in a small band about 110 kHz.

Warm alkali-metal vapor systems rival SQUIDs for the world's most sensitive magnetic field measurements [1]. Warm-atom systems hold several advantages for portable sensing, such as heated operation, rather than the cryogenic cooling and dewars required for SQUIDs. Miniature, high-performance atomic sensors are quickly becoming mature, aided by key innovations such as single-mode VCSELs and anodically bonded cells [2]. Commercial near-zero field atomic magnetometers show great promise for magnetically shielded magnetoencephalography (MEG) studies involving minor motion [3–5], using the popular spin-exchange relaxation free (SERF) atomic magnetometer [6]. However, SERF, and other styles of alkali magnetometers such as free-precession scalar, lose significant sensitivity at Earth's field and above due to effects that result from hyperfine coupling within the alkali atoms, such as spin-exchange relaxation [7] and heading errors [8, 9].

Portable free-precession atomic magnetometers have sufficient performance unshielded in Earth's field to detect MEG signals [10, 11], in addition to other various applications, due to their high dynamic range and linearity, resulting from frequency measurements ω of spins precessing due to a total magnetic field B . Here, calibration is provided by the gyromagnetic ratio $\gamma = \omega/B$ [12–15], rather than the voltage/field measurements of SERF and RF [16] sensors that require frequent calibration. Scalar magnetometers also demonstrate high performance within magnetic shielding, comparable to other precision modalities [17–19]. As such, there is high interest in developing methods to improve scalar magnetometer functionality [20], including introducing field modulations for vector sensing [21–23].

For precision magnetometry, it is common that sufficient buffer gas (above 50 torr N_2) is added to vapor cells for optical pumping efficiency, and slowing diffusive wall relaxation [24–29]. Here, absorption-line broadening is done for efficiency of both broad and narrow linewidth semiconductor lasers; for the former, broadening causes more absorption line overlap with a wide laser spectrum, and the latter so that all ground hyperfine states can be pumped. Trade-offs of broadening include lowered in-peak absorption efficiency, and lower maximum optical rotation by an incident linearly polarized probe beam [30]. We show careful probe tuning can assist optical pumping in low buffer gas pressure vapor cells, leading to high polarizations, while retaining large optical rotation for detection. We give a basic theory, and experimentally demonstrate high sensitivity and high bandwidth for scalar and RF magnetometers. Probe-assisted depopulation pumping also suppresses hyperfine coupling effects, such as heading error, and improves tolerance to large fields and inhomogeneous dephasing from magnetic gradients, important for a variety of applications of high-performance atomic magnetometry, such as MEG, magnetic navigation [31], and nEDM searches [32].

Scalar free-precession magnetometers are best operated by polarizing alkali atoms to unity into an edge state, maximizing SNR and providing T_2 extension by suppressing spin-exchange relaxation [8, 18]. Whether optical pumping occurs pulsed in a plane transverse to the measured scalar magnetic field B_0 , or is done longitudinally followed with a $\pi/2$ tipping pulse, a resulting transverse spin polarization will freely precesses about a total field B_0 , where light shifts are avoided with no pump laser during detection periods. The probe is tuned to maximize sensitivity, which is a trade-off of maximizing initial optical rotation while reducing probe broadening until it competes with the next largest rate (typically spin-exchange or wall relaxation). Increasing T_2 is beneficial to optimal sensitivity by roughly the measurement

* Contact author: limes.mark@gmail.com; Also at Bradley Department of Electrical and Computer Engineering

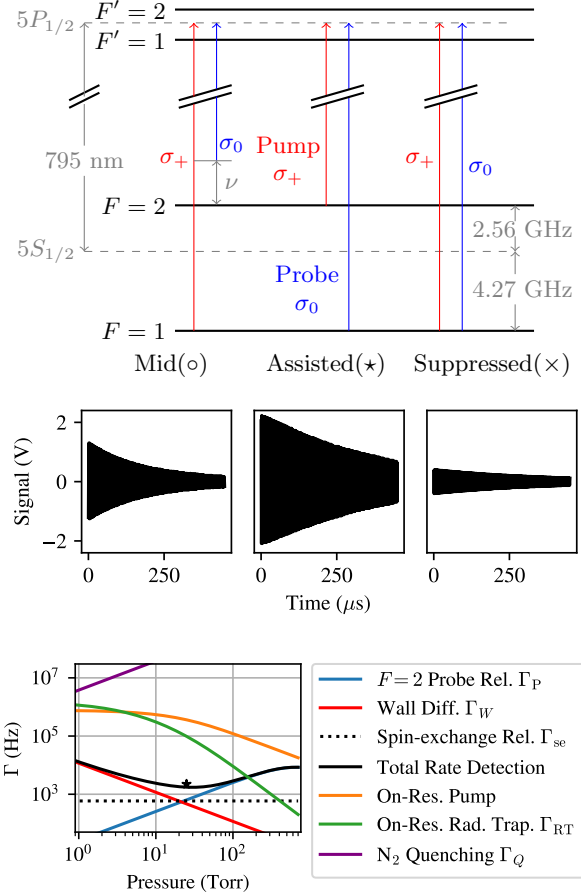


FIG. 1. (Top) Grotrian diagram for several regimes, along with representative data. (Bottom) Dominant rates for probe-assisted depopulation pumping; N_2 quenching overcomes radiative trapping, with (*) denoting experimental conditions being wall-relaxation and probe-broadening limited.

time T , which can be seen by converting the Cramér-Rao Lower Bound (CRLB) estimate of frequency noise [33, 34] to a field sensitivity

$$\delta B = \frac{\sqrt{12C}}{2\pi\gamma(A/\rho)T^{3/2}\sqrt{BW}} \left[\frac{T}{\sqrt{\text{Hz}}} \right], \quad (1)$$

with SNR A/ρ , integration time T , pulsed sensor bandwidth $BW = 1/2T_{\text{rep}}$, and C dependent on T_2 and T . Over a decay period, the average frequency of spin precession is proportional to the magnetic field through the low-field, strong hyperfine coupling gyromagnetic ratio γ (e.g. ⁸⁷Rb, $\gamma \approx 7$ GHz/T). To minimize Eq. 1, a single shot should last $\sim 2T_2$ [35]. Measurements are repeated every T_{rep} for a flat magnetometer bandwidth BW , with caveats—there are amplitude corrections required at higher in-band frequencies, and significant aliasing of out-of-band frequencies [36]. Artificially higher bandwidth magnetometers may be made by decreasing fitting windows, at a sensitivity loss linearly proportional to increasing bandwidth [37, 38].

At low buffer gas pressures for ⁸⁷Rb (below 100 Torr), $F = 2$ and $F = 1$ ground states can be addressed separately by narrow linewidth light [39, 40]. For this study, we are in a regime where narrow linewidth σ_+ pump light is efficient, but can only address either $F = 2$ or $F = 1$ at a given time. As shown by the assisted (★) regime in Fig. 1, an additional laser, such as a linearly polarized σ_0 transverse probe, can be tuned to simultaneously drive transitions from $F = 1$. While the σ_+ pump drives $F = 2$ states to the $m_F = 2$ edge state, an additional depopulation of $F = 1$ can achieve a maximum $\times 1.6$ enhancement in edge-stage polarization. After a pumping period, the linearly polarized probe tuned to $F = 1$ transitions is already conveniently detuned from the highly polarized $F = 2$ manifold by the $\Delta\nu = 6.8$ GHz hyperfine splitting, to provide high optical rotation with low magnetic linewidth probe broadening. For magnetometry, there are several advantages of probe-assisted depopulation pumping over high buffer gas operation, where the absorption lines of the hyperfine manifolds overlap. During detection, the probe also continuously depopulates $F = 1$, suppressing spin-exchange relaxation at high polarizations even in Earth-scale fields. Here, we are wall relaxation and probe broadening limited. Also, $F = 1$ contributes zero optical rotation, thus no frequency chirp from fast-decaying $F = 1$ states (precession ~ 1 kHz difference from $F = 2$ at 44 μT), leaving only non-linear Zeeman heading error effects [8, 41].

A model for probe-assisted depopulation pumping for free-precession magnetometry is made using absorption cross-section $\sigma = \pi r_e c f \text{Re}[V(\nu)]$ and optical rotation $\phi = lr_e c f n P_x \text{Im}[V(\nu)]/2$, with classical electron radius r_e , speed of light c , D_1 oscillator strength $f = 0.34$, path length l , alkali number density n , and P_x is polarization along the probe axis. We use Voigt profiles, as Doppler broadening $\Gamma_G = 0.57$ GHz is comparable to buffer-gas broadening $\Gamma_L \approx 18p/p_0$ GHz, with buffer gas pressure p , and $p_0 = 760$ Torr. For narrow laser linewidths, pumping rates are $\Gamma_P = \Phi\sigma$, with photon flux $\Phi = I_0/h\nu$. Small cells with very low buffer gas pressures (e.g. $\ll 1$ cc, 10 Torr) have large diffusive relaxation to walls, depolarizing atoms that can then contribute to radiation trapping [42]. The radiation trapping rate is estimated by $\Gamma_{RT} = K(M-1)f_{\text{spon}}\Gamma_P/2$ given in Ref. [42], where at 100°C, $K = 0.12$, $M = 28$ is the average number of times a photon is emitted before escaping the cell. We find a wide range of N_2 pressures are sufficient to provide non-radiative quenching, with greater than 10 MHz quenching rates Γ_Q , compared to on-resonance ~ 0.5 MHz pumping/radiation trapping rates. For diffusive wall relaxation, we use $\Gamma_W = [(\pi/L)^2 + (\mu/R)^2]D_0p_o/p$, with L and R cell length and radius, and diffusion coefficient D_0 for Rb in buffer gas [28]. Shown in Fig. 1, ~ 20 torr maximizes coherence time for probe-assisted depopulation pumping for our conditions; we also project a optimum sensitivity at this pressure of 8 ft/√Hz with 1.2 kHz bandwidth. Compare to high buffer gas broadening, where Voigt pro-

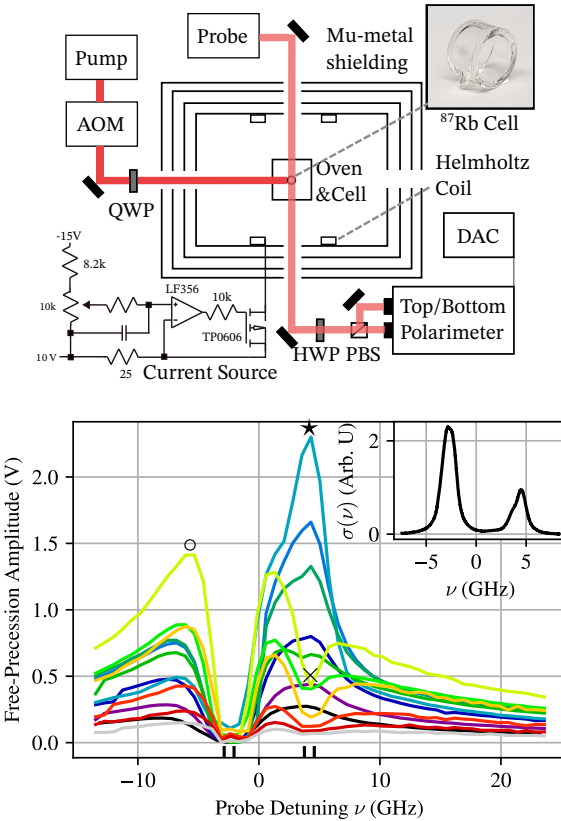


FIG. 2. (Top) Schematic of σ_+ light optically pumping a ^{87}Rb cell along a $44 \mu\text{T}$ field. After pumping periods, tipping pulses are applied, and spin precession is detected by optical rotation of a linearly polarized probe. (Bottom) For a 25 Torr buffer gas ^{87}Rb cell at 90°C , the scalar magnetometer amplitude responds to variation of probe and pump wavelengths. The probe detuning is shown along the x-axis, with pump detuning plotted from violet to red (low to high ν) in steps of 1.46 GHz. Labeled are mid (○), assisted (★), and suppressed (×) regimes, and a guide along the x-axis $F \rightarrow F' : 2 \rightarrow 1, 2 \rightarrow 2, 1 \rightarrow 1, 1 \rightarrow 1$. Inset: Linearly polarized probe absorption cross-section $\sigma(\nu)$.

files are replaced by complex Lorentzians and maximum optical rotation occurs with tuning $\nu_{\text{opt}} = \Gamma_L/2$; we also find optimal sensitivity δB increases as Γ_L when probe broadening Γ_P competes with buffer gas pressure independent rates Γ_{NP} , and bandwidth lowers with $1/\Gamma_L$.

For experiments, we use a ^{87}Rb vapor cell with two optical flats separated by 6 mm internal dimension and inner 10 mm diameter (0.47 cc), with 25 Torr of buffer gas, ratio 3:2 Ar:N₂. The cell is heated in a boron nitride oven with manganin wire driven by 80 kHz CW. Both pump and probe are Photodigm 795nm lasers with 0.5 MHz linewidth. We use 5-10 mW peak from each laser incident on the vapor cell. In Fig. 2, the pump light is fed into a InterAction Corp. Acousto-Optic Modulator (AOM), and circularly polarized by a quarter-wave plate (QWP). The probe beam passes through the cell's optical flats, and into a half-wave plate (HWP) and balanced po-

larimeter with polarizing beamsplitter cube (PBS), and a custom top-bottom polarimeter using split photodiodes. When balanced, 1 mW of light hits each of four photodiode regions. The photon-shot-noise limited signal is digitized with a National Instruments PXI-5922 card. To simulate Earth's field within magnetic shielding, a 40-turn Helmholtz coil is driven by a Libbrecht-Hall circuit [43]. The bias field and pump are applied along the cylinder axis, with probe transverse. After pumping, a resonant $\pi/2$ pulse is applied by a 4 cm square Helmholtz coil, placing spins on the transverse plane.

For a demonstration of probe-assisted depopulation pumping, wavelengths of both pump and probe are varied, and a single decay is recorded at 90°C . Fits to $A \exp(-t/T_2) \sin(\gamma B_0 t + \phi)$ extract amplitudes, which are plotted against probe tuning frequencies ν in steps of 0.73 GHz, and pump tuning plots vary by color from purple to red, in steps of 1.46 GHz (Fig. 2). When tuned directly on $F = 2$ ground state transitions, the linearly polarized probe is heavily absorbed and undergoes no optical rotation, leaving near-zero signal amplitude. For the mid (○) regime, we have probe tuning $\nu = -6$ GHz providing a moderate optical rotation signal, with pumping tuned to the $F = 1$ ground state transitions. When the probe is tuned to 4.27 GHz, there is an effective mechanism to depopulate the $F = 1$ manifold to the $F = 2$ ground states, such that a pump tuned to -2.56 GHz results in near unity polarization in the $F = 2$ manifold, as denoted by (★). Because the probe is already detuned by 6.8 GHz from $F = 2$, we also achieve high optical rotation and low probe broadening for detection. When the pump tuned to $F = 1$ at 4.27 GHz, a probe also tuned for $F = 1$ states counteracts any optical pumping to the $F = 2$ manifold, resulting in suppression (×) of signal. The response to laser tuning is robust with flipping pump light helicity and field, and remained similar across a range of Earth-scale fields (5 to 150 μT). To confirm cell pressures, the incident linearly polarized probe power is decreased to 0.5 mW, and transmission converted to absorption cross-section $\sigma(\nu)$ by $I = I_0 \exp(-n\sigma(\nu)l)$, with I/I_0 the output/input light intensity, number density n , and $l = 6$ mm path length through cell (Fig. 2 Inset). The absorption cross-section $\sigma(\nu)$ is fit to four Voigt profiles, for each hyperfine ground to excited transition, giving pressure broadening of $\Gamma_B = 0.59 \pm 0.02$ GHz, for 25 ± 1 Torr of Ar:N₂ [44].

To demonstrate sensitivity, lasers are tuned for the probe-assisted depopulation pumping regime. The probe detection is split to detect vapor cell top and bottom [45] and optical rotation signals are captured, shown in Fig. 3. The shot-to-shot repetition rate is 2 kHz, with the detection period 0.4 ms each shot and $T_2 = 0.33$ ms. Separate shots are fit to decaying sine waves using a non-linear fitting routine, where magnetic fields are extracted by $B = \gamma/\omega$. The raw magnetometer performance of roughly $200 \text{ fT}/\sqrt{\text{Hz}}$ is limited by the Libbrecht-Hall supply noise, demonstrated by the roughly $\times 5$ lower gradiometer sensitivity of $35.7 \pm 0.3 \Delta \text{fT}/\sqrt{\text{Hz}}$ (injecting

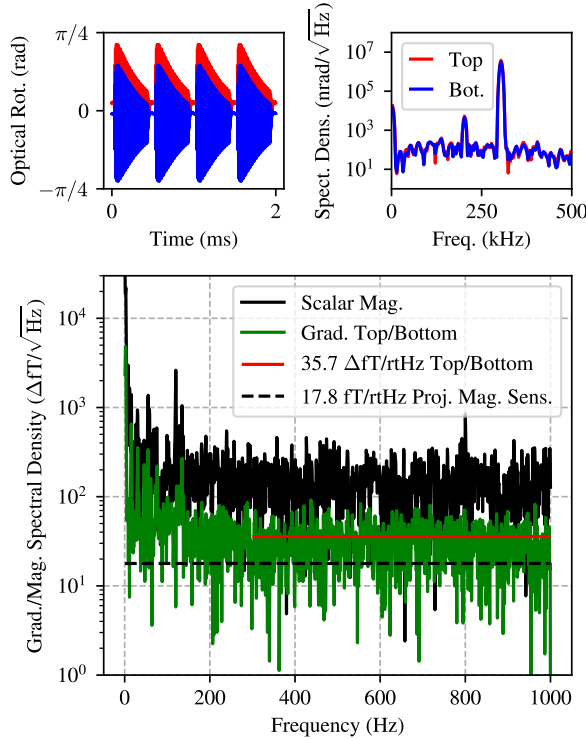


FIG. 3. Top/bottom optical rotation and spectral densities for 0.4 ms shots are shown. Frequencies are extracted each shot for vapor cell top/bottom, and repeated with 2 kHz. A probe-assisted depopulation pumping scalar magnetometer measures 44 μ T with current supply noise 200 fT/ $\sqrt{\text{Hz}}$. Top/bottom gradiometry projects magnetic field sensitivity of 17.8 ± 0.3 fT/ $\sqrt{\text{Hz}}$ with 1 kHz bandwidth.

broadband noise of $1 \text{ nT}/\sqrt{\text{Hz}}$ indicates a gradiometer common mode rejection ratio of ~ 3000). Gradiometry projects that a magnetometer formed from recombining the cell top and bottom has a sensitivity of $18 \text{ fT}/\sqrt{\text{Hz}}$. While other methods have sensitivities degrade significantly above Earth's field, see [10, 34, 41], we observe no field dependence between 10-100 μ T. Moreover, we retain high sensitivity with large bandwidth using less than $\pi/4$ optical rotation. Achieving higher bandwidth by means that do not degrade sensitivity is important for gradient tolerance (and single-shot frequency error requirements), e.g. from Ref. [34], a similar cell size of 0.5 cc with high buffer gas, and multi-pass probe, yields $14 \text{ fT}/\sqrt{\text{Hz}}$ with 90 Hz bandwidth—our 1 kHz bandwidth requires a factor $\times 10$ less measurement time per shot. Here gradient relaxation through diffusion is low compared to inhomogeneous T_2^* dephasing, so there is a proportional gain in gradient tolerance with decreasing measurement time $dB/dz = \Delta\phi/(\gamma LT)$, e.g., a signal height loss of $\text{sinc}(\Delta\phi) = 1/e$ results from $160 \text{ nT}/\text{cm}$ over 0.4 ms, or $16 \text{ nT}/\text{cm}$ in 4 ms. The measured gradiometer is higher than the Eq. 1 CRLB estimate of $27.2 \text{ fT}/\sqrt{\text{Hz}}$ for observed SNR and T_2 , with magnetometer of $13.6 \text{ fT}/\sqrt{\text{Hz}}$.

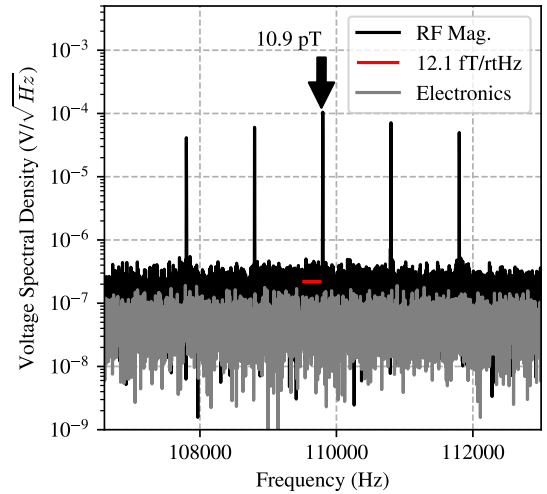


FIG. 4. An RF magnetometer is made with the same geometry as the scalar sensor, where the resonant frequency is determined by the 15.7 μ T scalar field strength.

The same method and geometry can be used for RF magnetometry, which we show experimentally with cell temperature increased to 130°C and continuous probe-assisted depopulation pumping [16, 46, 47]. To calibrate test fields, the bias field B_0 is tuned for resonance near 110 kHz, and Rabi oscillations are driven within the rotating wave approximation where the driving field B_1 is much less than B_0 . In Fig. 4, we extract a magnetic field sensitivity of $12.1 \pm 0.4 \text{ fT}/\sqrt{\text{Hz}}$. Five separate frequencies detected around 110 kHz are shown with amplitude 10.9 pT, yielding a magnetometer full-width half-max of roughly 3 kHz. The spin-projection noise limit is given by $\delta B = (1/\gamma)\sqrt{8/(F_z n V T_2)}$ where F_z is polarization along z , n is number density, and V is volume probed; for our parameters we find δB is below $10 \text{ fT}/\sqrt{\text{Hz}}$.

We demonstrated probe-assisted depopulation pumping for scalar and RF magnetometry in low buffer gas alkali vapor cells. The small cell size and low-power, single-pass lasers used give an important proof-of-principle for compact, portable sensor heads using low-pressure vapor cells for improved gradient tolerance and retention of sensitivity in large Earth-scale fields. The suppression of hyperfine effects opens up a new regime for precision magnetometry, including SERF extensions [48]; for example, a ^{87}Rb 50% polarized $F = 2$ manifold can be strongly probed with tuning at $F = 1$ ($\Delta\nu = 6.8 \text{ GHz}$); here the spin evolution due to a magnetic field will only have $F = 2$ character. In addition, this method is valid for the other popular alkali metals for precision magnetometry, K and Cs. To improve raw sensitivity, a multi-pass configuration may also be used, for spin-noise limited operation [17, 34, 49–53].

We thank the Virginia Tech Office of Research and Innovation for support and Brian Saam for discussions.

-
- [1] H. Dang, A. C. Maloof, and M. V. Romalis, Ultrahigh sensitivity magnetic field and magnetization measurements with an atomic magnetometer, *Applied physics letters* **97** (2010).
- [2] J. Kitching, Chip-scale atomic devices, *Applied Physics Reviews* **5**, 031302 (2018).
- [3] C. N. Johnson, P. D. D. Schwindt, and M. Weisend, Multi-sensor magnetoencephalography with atomic magnetometers, *Physics in Medicine and Biology* **58**, 6065 (2013).
- [4] E. Boto, N. Holmes, T. M. Tierney, J. Leggett, R. Hill, S. Mellor, G. Roberts, G. Barnes, R. Bowtell, M. Brookes, *et al.*, Magnetoencephalography using optically pumped magnetometers, *Fifty Years of Magnetoencephalography*. Oxford University Press, New York , 104 (2020).
- [5] O. Alem, K. J. Hughes, I. Buard, T. P. Cheung, T. Maydew, A. Griesshammer, K. Holloway, A. Park, V. Lechuga, C. Coolidge, M. Gerginov, E. Quigg, A. Seames, E. Kronberg, P. Teale, and S. Knappe, An integrated full-head opm-meg system based on 128 zero-field sensors, *Frontiers in Neuroscience* **Volume 17 - 2023**, 10.3389/fnins.2023.1190310 (2023).
- [6] J. C. Allred, R. N. Lyman, T. W. Kornack, and M. V. Romalis, High-sensitivity atomic magnetometer unaffected by spin-exchange relaxation, *Phys. Rev. Lett.* **89**, 130801 (2002).
- [7] W. Happer and A. C. Tam, Effect of rapid spin exchange on the magnetic-resonance spectrum of alkali vapors, *Phys. Rev. A* **16**, 1877 (1977).
- [8] W. Lee, V. G. Lucivero, M. V. Romalis, M. E. Limes, E. L. Foley, and T. W. Kornack, Heading errors in all-optical alkali-metal-vapor magnetometers in geomagnetic fields, *Phys. Rev. A* **103**, 063103 (2021).
- [9] D. P. Hewatt, M. Ellmeier, C. Kiehl, T. S. Menon, J. W. Pollock, C. A. Regal, and S. Knappe, Investigating the hyperfine systematic error and relative phase in low-spin-polarization alkali-metal free-induction-decay magnetometers, *Phys. Rev. A* **111**, 033106 (2025).
- [10] M. Limes, E. Foley, T. Kornack, S. Caliga, S. McBride, A. Braun, W. Lee, V. Lucivero, and M. Romalis, Portable magnetometry for detection of biomagnetism in ambient environments, *Phys. Rev. Appl.* **14**, 011002 (2020).
- [11] R. J. Clancy, V. Gerginov, O. Alem, S. Becker, and S. Knappe, A study of scalar optically-pumped magnetometers for use in magnetoencephalography without shielding, *Physics in Medicine and Biology* **66**, 175030 (2021).
- [12] D. Sheng, A. R. Perry, S. P. Krzyzewski, S. Geller, J. Kitching, and S. Knappe, A microfabricated optically-pumped magnetic gradiometer, *Applied Physics Letters* **110**, 031106 (2017).
- [13] V. Gerginov, S. Krzyzewski, and S. Knappe, Pulsed operation of a miniature scalar optically pumped magnetometer, *J. Opt. Soc. Am. B* **34**, 1429 (2017).
- [14] A. R. Perry, M. D. Bulatowicz, M. Larsen, T. G. Walker, and R. Wyllie, All-optical intrinsic atomic gradiometer with sub-20 ft/cm/ $\sqrt{\text{hz}}$ sensitivity in a 22 μt earth-scale magnetic field., *Optics Express* **28**, 36696 (2020), <https://doi.org/10.1364/oe.408486>.
- [15] V. Gerginov, M. Pomponio, and S. Knappe, Scalar magnetometry below 100 ft/hz $^{1/2}$ in a microfabricated cell, *IEEE Sensors Journal* **20**, 12684 (2020).
- [16] I. M. Savukov, S. J. Seltzer, M. V. Romalis, and K. L. Sauer, Tunable atomic magnetometer for detection of radio-frequency magnetic fields, *Phys. Rev. Lett.* **95**, 063004 (2005).
- [17] S. Li, P. Vachaspati, D. Sheng, N. Dural, and M. V. Romalis, Optical rotation in excess of 100 rad generated by rb vapor in a multipass cell, *Phys. Rev. A* **84**, 061403 (2011).
- [18] D. Sheng, S. Li, N. Dural, and M. V. Romalis, Subfemtotesla scalar atomic magnetometry using multipass cells, *Phys. Rev. Lett.* **110**, 160802 (2013).
- [19] V. Lucivero, W. Lee, M. Limes, E. Foley, T. Kornack, and M. Romalis, Femtotesla nearly-quantum-noise-limited pulsed gradiometer at earth-scale fields, *Phys. Rev. Appl.* **18**, L021001 (2022).
- [20] D. Hunter, M. S. Mrozowski, A. McWilliam, S. J. Ingleby, T. E. Dyer, P. F. Griffin, and E. Riis, Optical pumping enhancement of a free-induction-decay magnetometer, *J. Opt. Soc. Am. B* **40**, 2664 (2023).
- [21] E. Alexandrov, M. Balabas, V. Kulyasov, A. Ivanov, A. Pazgalev, J. Rasson, A. Vershovski, and N. Yakobson, Three-component variometer based on a scalar potassium sensor, *Measurement Science and Technology* **15**, 918 (2004).
- [22] A. Vershovskii, M. Balabas, A. Ivanov, V. Kulyasov, A. Pazgalev, and E. Aleksandrov, Fast three-component magnetometer-variometer based on a cesium sensor, *Technical Physics* **51**, 112 (2006).
- [23] T. Wang, W. Lee, M. Limes, T. Kornack, E. Foley, and M. Romalis, Pulsed vector atomic magnetometer using an alternating fast-rotating field, *Nature communications* **16**, 1374 (2025).
- [24] C. Ottinger, R. Scheps, G. York, and A. Gallagher, Broadening of the rb resonance lines by the noble gases, *Physical Review A* **11**, 1815 (1975).
- [25] M. D. Rotondaro and G. P. Perram, Collisional broadening and shift of the rubidium d1 and d2 lines (52s12 \rightarrow 52p12, 52p32) by rare gases, h2, d2, n2, ch4 and cf4, *Journal of Quantitative Spectroscopy and Radiative Transfer* **57**, 497 (1997).
- [26] M. Romalis, E. Miron, and G. Cates, Pressure broadening of rb d 1 and d 2 lines by 3 he, 4 he, n 2, and xe: Line cores and near wings, *Physical Review A* **56**, 4569 (1997).
- [27] M. Erhard, S. Nußmann, and H. Helm, Power broadening and doppler effects of coherent dark resonances in rb, *Phys. Rev. A* **62**, 061802 (2000).
- [28] W. Happer, Y.-Y. Jau, and T. Walker, *Optically pumped atoms* (John Wiley & Sons, 2010).
- [29] G. Oelsner, R. IJsselssteijn, T. Scholtes, A. Krüger,

- V. Schultze, G. Seyffert, G. Werner, M. Jäger, A. Chwala, and R. Stolz, Integrated optically pumped magnetometer for measurements within earth's magnetic field, *Phys. Rev. Appl.* **17**, 024034 (2022).
- [30] W. Happer and B. Mathur, Off-resonant light as a probe of optically pumped alkali vapors, *Physical Review Letters* **18**, 577 (1967).
- [31] J. S. Bennett, B. E. Vyhalek, H. Greenall, E. M. Bridge, F. Gotardo, S. Forstner, G. I. Harris, F. A. Miranda, and W. P. Bowen, Precision magnetometers for aerospace applications: A review, *Sensors* **21**, 5568 (2021).
- [32] C. Abel, S. Afach, N. J. Ayres, G. Ban, G. Bison, K. Bodek, V. Bondar, E. Chanel, P.-J. Chiu, C. B. Crawford, Z. Chowdhuri, M. Daum, S. Emmenegger, L. Ferraris-Bouchez, M. Fertl, B. Franke, W. C. Griffith, Z. D. Grujić, L. Hayen, V. Hélaine, N. Hild, M. Kasprzak, Y. Kermaidic, K. Kirch, P. Knowles, H.-C. Koch, S. Komposch, P. A. Koss, A. Kozela, J. Kremppel, B. Lauss, T. Lefort, Y. Lémière, A. Leredde, A. Mtchedlishvili, P. Mohanmurthy, M. Musgrave, O. Naviliat-Cuncic, D. Pais, A. Pazgalev, F. M. Piegsa, E. Pierre, G. Pignol, P. N. Prashanth, G. Quéméner, M. Rawlik, D. Rebreyend, D. Ries, S. Rocca, D. Rozpedzik, P. Schmidt-Wellenburg, A. Schnabel, N. Severijns, R. T. Dinani, J. Thorne, A. Weis, E. Wursten, G. Wyszynski, J. Zejma, and G. Zsigmond, Optically pumped cs magnetometers enabling a high-sensitivity search for the neutron electric dipole moment, *Phys. Rev. A* **101**, 053419 (2020).
- [33] R. J. Hoare, E. R. Oteiza, and T. E. Chupp, The search for a permanent electric dipole moment using ^{129}Xe and ^{3}He , in *AIP Conference Proceedings*, Vol. 275 (American Institute of Physics, 1993) pp. 73–84.
- [34] V. Lucivero, W. Lee, N. Dural, and M. Romalis, Femtotesla direct magnetic gradiometer using a single multipass cell, *Physical Review Applied* **15**, 014004 (2021).
- [35] M. Limes, N. Dural, M. Romalis, E. Foley, T. Kornack, A. Nelson, and L. Grisham, Long spin-1/2 noble gas coherence times in mm-sized anodically bonded batch-fabricated ^{3}He - ^{129}Xe - ^{87}Rb cells, *Applied Physics Letters* **126** (2025).
- [36] M. E. Limes, L. Rathbun, E. Foley, T. Kornack, Z. Hainsel, and A. Braun, Frequency-dependent amplitude correction to free-precession scalar magnetometers, *IEEE Sensors Letters* **9**, 1 (2025).
- [37] N. Wilson, C. Perrella, R. Anderson, A. Luiten, and P. Light, Wide-bandwidth atomic magnetometry via instantaneous-phase retrieval, *Phys. Rev. Res.* **2**, 013213 (2020).
- [38] A. Jaufenthaler, T. Kornack, V. Lebedev, M. E. Limes, R. Körber, M. Liebl, and D. Baumgarten, Pulsed optically pumped magnetometers: Addressing dead time and bandwidth for the unshielded magnetorelaxometry of magnetic nanoparticles, *Sensors* **21**, 10.3390/s21041212 (2021).
- [39] T. McClelland, L. Lam, and T. Kwon, Anomalous narrowing of magnetic-resonance linewidths in optically pumped alkali-metal vapors, *Physical Review A* **33**, 1697 (1986).
- [40] J. Dreiling, E. Norrgard, D. Tupa, and T. J. Gay, Transverse measurements of polarization in optically pumped rb vapor cells, *Physical Review A—Atomic, Molecular, and Optical Physics* **86**, 053416 (2012).
- [41] R. Zhang, D. Kanta, A. Wickenbrock, H. Guo, and D. Budker, Heading-error-free optical atomic magnetometry in the earth-field range, *Phys. Rev. Lett.* **130**, 153601 (2023).
- [42] M. A. Rosenberry, J. P. Reyes, D. Tupa, and T. J. Gay, Radiation trapping in rubidium optical pumping at low buffer-gas pressures, *Phys. Rev. A* **75**, 023401 (2007).
- [43] K. Libbrecht and J. L. Hall, A low-noise high-speed diode laser current controller, *Review of scientific instruments* **64**, 2133 (1993).
- [44] M. Ardit and T. Carver, Hyperfine relaxation of optically pumped rb 87 atoms in buffer gases, *Physical Review* **136**, A643 (1964).
- [45] I. K. Kominis, T. W. Kornack, J. C. Allred, and M. V. Romalis, A subfemtotesla multichannel atomic magnetometer, *Nature* **422**, 596 (2003).
- [46] I. Savukov, T. Karaulanov, and M. G. Boshier, Ultra-sensitive high-density rb -87 radio-frequency magnetometer, *Applied Physics Letters* **104**, 023504 (2014).
- [47] R. J. Cooper, D. W. Prescott, P. Matz, K. L. Sauer, N. Dural, M. V. Romalis, E. L. Foley, T. W. Kornack, M. Monti, and J. Okamitsu, Atomic magnetometer multi-sensor array for rf interference mitigation and unshielded detection of nuclear quadrupole resonance, *Physical Review Applied* **6**, 064014 (2016).
- [48] A. Berrebi, M. Dikopoltsev, O. Katz, and O. Katz, Optical protection of alkali-metal atoms from spin relaxation, *Phys. Rev. Lett.* **135**, 023201 (2025).
- [49] M. Romalis and T. Kornack, *Scalar Multi-Pass Atomic Magnetometer*, Tech. Rep. (2017).
- [50] Y. Liu, X. Peng, H. Wang, B. Wang, K. Yi, D. Sheng, and H. Guo, Femtotesla 4 He magnetometer with a multipass cell, *Optics Letters* **47**, 5252 (2022).
- [51] S.-Q. Liu, Q.-Q. Yu, H. Zhou, and D. Sheng, Sensitive and stable atomic vector magnetometer to detect weak fields using two orthogonal multipass cavities, *Physical Review Applied* **19**, 044062 (2023).
- [52] K. Yi, Y. Liu, B. Wang, W. Xiao, D. Sheng, X. Peng, and H. Guo, Free-induction-decay 4 He magnetometer using a multipass cell, *Physical Review Applied* **22**, 014084 (2024).
- [53] D. Heilman, K. Sauer, D. Prescott, C. Motamedi, N. Dural, M. Romalis, and T. Kornack, Large-scale multipass two-chamber rf atomic magnetometer, *Physical Review Applied* **22**, 054024 (2024).